crystals

MDPI

Article

Evolution of Phase Transformation on Microwave Dielectric Properties of $BaSi_xO_{1+2x}$ Ceramics and Their Temperature-Stable LTCC Materials

Tailai Wen [1,2], Yulu Luo [1], Zehang Zeng [1], Xiaotian Liu [1], Changzhi Yin [3], Yiyang Cai [3], Xiaoxiao Li [4], Kang Du [1,2,5,*], Wen Lei [3,4,*] and Shengxiang Wang [1,2,5,*]

1 School of Mathematical and Physical Sciences, Wuhan Textile University, Wuhan 430200, China
2 School of Electronic and Electrical Engineering, Wuhan Textile University, Wuhan 430200, China
3 Key laboratory of Functional Materials for Electronic Information (B) of MOE, School of Optical and Electronic Information, Huazhong University of Science and Technology, Wuhan 430074, China
4 Wenzhou Key Laboratory of Microwave Communication Materials and Devices, Wenzhou Advanced Manufacturing Institute of HUST, Wenzhou 325035, China
5 State Key Laboratory of New Textile Materials and Advanced Processing Technologies, Wuhan Textile University, Wuhan 430200, China
* Correspondence: dk@wtu.edu.cn (K.D.); wenlei@mail.hust.edu.cn (W.L.); shxwang@wtu.edu.cn (S.W.)

Abstract: $BaSi_xO_{1+2x}$ ($1.61 \leq x \leq 1.90$) and LiF-doped $BaSi_{1.63}O_{4.26}$ ceramics were prepared by using a traditional solid-state method at the optimal sintering temperatures. The evolution of phase compositions of $BaSi_xO_{1+2x}$ ($1.61 \leq x \leq 1.9$) ceramics was revealed. The coexistence of $Ba_5Si_8O_{21}$ and $Ba_3Si_5O_{13}$ phases was obtained in $BaSi_xO_{1+2x}$ ($1.61 \leq x \leq 1.67$) ceramics. The $BaSi_2O_5$ phase appeared in$BaSi_xO_{1+2x}$ ($1.68 \leq x \leq 1.90$) ceramics. At $1.68 \leq x \leq 1.69$, only $BaSi_2O_5$ and $Ba_3Si_5O_{13}$ phases existed. With the further increase in x, the $Ba_5Si_8O_{21}$ phase appeared, and $BaSi_2O_5$, $Ba_5Si_8O_{21}$ and $Ba_3Si_5O_{13}$ phases coexisted in $BaSi_xO_{1+2x}$ ($1.70 \leq x \leq 1.90$) ceramics. The phase compositions of $BaSi_xO_{1+2x}$ ($1.61 \leq x \leq 1.90$) ceramics were controlled by the ratio of Ba:Si. The $BaSi_xO_{1+2x}$ ($x = 1.68$) ceramics with 98.15 wt% $Ba_3Si_5O_{13}$ and 1.85 wt% $BaSi_2O_5$ phases exhibited a negative τ_f value (-37.53 ppm/°C), and the good microwave dielectric properties of $\varepsilon_r = 7.51$, $Q \times f = 13{,}038$ GHz and $\tau_f = +3.95$ ppm/°C were obtained for $BaSi_{1.63}O_{4.26}$ ceramics with 70.05 wt% $Ba_5Si_8O_{21}$ and 29.95 wt% $Ba_3Si_5O_{13}$ phases. The addition of LiF sintering aids were able to reduce the sintering temperatures of $BaSi_{1.63}O_{4.26}$ ceramics to 800 °C. The phase composition of $BaSi_{1.63}O_{4.26}$ ceramics was affected by the sintering temperature, and the coexistence of $Ba_5Si_8O_{21}$, $Ba_2Si_3O_8$, $BaSi_2O_5$ and SiO_2 phases was achieved in $BaSi_{1.63}O_{4.26}$-3 wt% LiF ceramics. The $BaSi_{1.63}O_{4.26}$-3 wt% LiF ceramics sintered at 800 °C exhibited dense microstructures and excellent microwave dielectric properties ($\varepsilon_r = 7.10$, $Q \times f = 12{,}463$ GHz and $\tau_f = +5.75$ ppm/°C), and no chemical reaction occurred between $BaSi_{1.63}O_{4.26}$-3 wt% LiF ceramics and the Ag electrodes, which indicates their potential for low-temperature co-fired ceramic (LTCC) applications.

Keywords: barium silicate; phase composition; microwave dielectric property; low-temperature co-fired ceramic application

check for updates

Citation: Wen, T.; Luo, Y.; Zeng, Z.; Liu, X.; Yin, C.; Cai, Y.; Li, X.; Du, K.; Lei, W.; Wang, S. Evolution of Phase Transformation on Microwave Dielectric Properties of $BaSi_xO_{1+2x}$ Ceramics and Their Temperature-Stable LTCC Materials. *Crystals* **2023**, *13*, 870. https://doi.org/10.3390/cryst13060870

Academic Editor: Francisco M. Morales

Received: 8 May 2023
Revised: 22 May 2023
Accepted: 24 May 2023
Published: 26 May 2023

Copyright: © 2023 by the authors. Licensee MDPI, Basel, Switzerland. This article is an open access article distributed under the terms and conditions of the Creative Commons Attribution (CC BY) license (https://creativecommons.org/licenses/by/4.0/).

1. Introduction

The rapid development of telecommunication has promoted the high demand for multi-layer devices and microwave dielectric ceramics [1–5]. Barium silicates with excellent luminescence and dielectric properties are widely used in optical glasses and microwave dielectric ceramics [6–12]. The low cost and free of variable valence elements of barium silicates indicated their great application potential, especially in communication applications [13,14]. The Si–O bond was also strong because it is approximately 55% covalent and 45% ionic [15–17]. Barium silicates with high contents of SiO_4 tetrahedra and Si–O bonds

demonstrated their low permittivity (ε_r < 15) and high-quality factor ($Q \times f$), which attracted considerable attention regarding microwave dielectric materials [18–22]. However, 13 crystalline phases were known in the BaO–SiO_2 system [23], which indicates that the complex phase compositions might exist in barium silicates. Ambiguous phase compositions might limit the application of barium silicates in microwave dielectric materials.

The microwave dielectric properties of barium silicates were first reported by Wen Lei et al. [9], and a $BaSi_2O_5$ ceramic with excellent microwave dielectric properties (ε_r = 6.7, $Q \times f$ = 59,500 GHz and τ_f = −28.0 ppm/°C) was synthesised through sintering at 1250 °C. Enzhu Li et al. pointed out that the synthesis temperature of a single-phase $BaSi_2O_5$ ceramic was more than 1100 °C, and the coexistence of $BaSi_2O_5$, $Ba_5Si_8O_{21}$ ($BaSi_{1.6}O_{4.2}$) and SiO_2 phases was identified in $BaSi_2O_5$ ceramics. The $Ba_5Si_8O_{21}$ phases existed in $BaSi_2O_5$-2 wt% Li_2O–B_2O_3–CaO–CuO glass ceramics when their sintering temperature was below 800 °C, which means that the $Ba_5Si_8O_{21}$ phase was easier to synthesise than the $BaSi_2O_5$ phase [10]. A single-phase $BaSi_2O_5$ ceramic sintered at 1225 °C was prepared by Yun Zhang [11]. The $Ba_5Si_8O_{21}$ ceramic with a stable phase composition and novel positive temperature coefficient of the resonance frequency (τ_f) was used as a τ_f regulator to control the negative τ_f values of many low-ε_r microwave dielectric ceramics [12]. The $Ba_5Si_8O_{21}$ ceramics always exhibited the $Ba_5Si_8O_{21}$ phase at a high sintering temperature (above 800 °C). However, the $Ba_3Si_5O_{13}$ ($BaSi_{1.667}O_{4.334}$) ceramic, as an intermediate compound between $Ba_5Si_8O_{21}$ ($BaSi_{1.6}O_{4.2}$) and $BaSi_2O_5$, exhibited the highest structural and topological complexity in barium silicates [8]. The $Ba_3Si_5O_{13}$ ($BaSi_{1.667}O_{4.334}$) ceramics sintering at different temperatures exhibited the opposite τ_f values (+37.0 ppm/°C sintering at 1200 °C and −36.0 ppm/°C sintering at 1250 °C) and different phase compositions ($Ba_5Si_8O_{21}$ and $BaSi_2O_5$ phases sintered at 1200 °C and $Ba_3Si_5O_{13}$ phase sintered at 1250 °C) [9]. Toshihiro Moriga et al. pointed out that $Ba_3Si_5O_{13}$ single-phase ceramics sintered at 1000 °C could be synthesised at stoichiometric ratios [7]. The small difference in the Ba:Si ratios of the $Ba_5Si_8O_{21}$, $Ba_3Si_5O_{13}$ and $BaSi_2O_5$ phases caused difficulty in synthesizing $Ba_3Si_5O_{13}$ ceramics.

Considering the excellent application potential of barium silicate ceramics in LTCC technology, the variation in the phase compositions of $BaSi_xO_{1+2x}$ ceramics with stoichiometric ratios and sintering temperatures needs to be investigated. This study aimed to clarify the phase compositions of $BaSi_xO_{1+2x}$ ($1.61 \leq x \leq 1.9$) ceramics with different stoichiometric ratios and investigate the evolution of their phase compositions on microwave dielectric properties. Simultaneously, high-performance $BaSi_xO_{1+2x}$-based LTCC materials with LiF doped were prepared.

2. Materials and Methods

$BaSi_xO_{1+2x}$ ($1.61 \leq x \leq 1.9$)- and LiF-doped $BaSi_xO_{1+2x}$ ceramics were prepared using the solid reaction method. $BaCO_3$ (99.9%), SiO_2 (99.9%) and LiF (99.9%) were weighed according to the stoichiometric formulation of $BaSi_xO_{1+2x}$ ($1.61 \leq x \leq 1.9$) and ground in deionised water for 5 h. After drying, $BaSi_xO_{1+2x}$-prepared powders were calcined at 1050 °C for 5 h to obtain barium silicates. After being re-milled for 5 h and dryed, the as-prepared powders together with 8 wt% PVA were pressed into cylindrical samples. The $BaSi_xO_{1+2x}$ samples were then sintered at 1300–1325 °C for 5 h. The $BaSi_xO_{1+2x}$ calcined powders and LiF were weighed according to the mass percentage formulation of $BaSi_xO_{1+2x}$-y wt% LiF ($1 \leq y \leq 3$), which were sintered at 800–1025 °C for 3 h.

The sintered samples of $BaSi_xO_{1+2x}$ and $BaSi_xO_{1+2x}$-y wt% LiF ($1 \leq y \leq 3$) ceramics were broken up and ground into powders. The phase and crystal structure of powders were obtained using an X-ray diffractometer (X'Pert PRO). The Rietveld refinement of samples was conducted via Fullprof software [24]. The polished surfaces of samples were observed via scanning electron microscopy (SEM; Sirion 200) after thermal etching. The microwave dielectric properties of as-sintered $BaSi_xO_{1+2x}$ ($1.61 \leq x \leq 1.9$) and $BaSi_xO_{1+2x}$-y wt% LiF ($1 \leq y \leq 3$) ceramics were measured in the range of 10–14 GHz by employing the Hakki–Coleman methods with a network analyser (Keysight E5063A) [25].

3. Results

The $BaSi_xO_{1+2x}$ ($1.61 \leq x \leq 1.90$) ceramics at the optimal sintering temperature (T_{sint}) were broken up and ground into powders for X-ray analysis. As shown in Figure 1a, the optimal sintering temperature of $BaSi_xO_{1+2x}$ ($1.61 \leq x \leq 1.67$) ceramics was between 1300 and 1325 °C. Only $Ba_5Si_8O_{21}$ phase seemed to exist in $BaSi_xO_{1+2x}$ ($1.61 \leq x \leq 1.62$) ceramics, and the $BaSi_xO_{1+2x}$ ($1.66 \leq x \leq 1.67$) ceramics exhibited the $Ba_3Si_5O_{13}$ single phase. The evident coexistence of $Ba_5Si_8O_{21}$ and $Ba_3Si_5O_{13}$ phases was observed in $BaSi_xO_{1+2x}$ ($1.63 \leq x \leq 1.65$) ceramics. As illustrated in Figure 1c, the $Ba_3Si_5O_{13}$ single phase existed in the $BaSi_xO_{1+2x}$ (x = 1.68) ceramics, and the obvious coexistence of $Ba_3Si_5O_{13}$ and $BaSi_2O_5$ phases was observed in the $BaSi_xO_{1+2x}$ ($1.69 \leq x \leq 1.90$) ceramics. However, the similar XRD patterns between $Ba_3Si_5O_{13}$ and $Ba_5Si_8O_{21}$ phases caused difficulty in distinguishing the phase compositions of $BaSi_xO_{1+2x}$ ceramics. The enlarged XRD patterns of $BaSi_xO_{1+2x}$ ($1.61 \leq x \leq 1.9$) ceramics at a 20°–30° scanning range can be seen in Figure 1b,d, along with the evolution of the main XRD peaks. The evident $Ba_3Si_5O_{13}$ second phase existed in $BaSi_xO_{1+2x}$ (x = 1.62) ceramics, and the content of the $Ba_3Si_5O_{13}$ phase in $BaSi_xO_{1+2x}$ ($1.61 \leq x \leq 1.67$) ceramics increased gradually with the rise in x. In the $BaSi_xO_{1+2x}$ (x = 1.67) ceramics, the $Ba_5Si_8O_{21}$ second phase was present. The single-phase $Ba_3Si_5O_{13}$ ceramics might be seen in the $BaSi_xO_{1+2x}$ (x = 1.68) ceramics (Figure 1d). With the further increase in x, the intensity of the XRD patterns of the $BaSi_2O_5$ and $Ba_3Si_5O_{13}$ phases gradually rose and decreased, respectively. The evident $Ba_5Si_8O_{21}$ phase also existed in $BaSi_xO_{1+2x}$ ($1.80 \leq x \leq 1.85$) ceramics, which indicates the complex evolution of the phase compositions of $BaSi_xO_{1+2x}$ ($1.68 \leq x \leq 1.90$) ceramics. Moreover, the $Ba_3Si_5O_{13}$ ceramics were able to be synthesised via sintering at 1325 °C.

The Rietveld refinement of $BaSi_xO_{1+2x}$ ($1.61 \leq x \leq 1.90$) ceramics was conducted for quantitative analysis via phase composition. The results of the Rietveld refinement are shown in Table 1, and the calculated XRD patterns of $BaSi_xO_{1+2x}$ ($1.61 \leq x \leq 1.90$) ceramics matched the measured XRD patterns well (Figure 2). Therefore, the fitting content of phase compositions was accurate. As shown in Table 1, the $Ba_5Si_8O_{21}$ main phase and $Ba_3Si_5O_{13}$ second phase existed in $BaSi_xO_{1+2x}$ ($1.61 \leq x \leq 1.64$) ceramics. The main phase in $BaSi_xO_{1+2x}$ ($1.65 \leq x \leq 1.67$) ceramics changed from the $Ba_5Si_8O_{21}$ to $Ba_3Si_5O_{13}$ phase. Moreover, the $Ba_5Si_8O_{21}$ second phase changed to the $BaSi_2O_5$ phase in the $BaSi_xO_{1+2x}$ (x = 1.68) ceramics. The $BaSi_xO_{1+2x}$ (x = 1.68) ceramics with 98.5 wt% $Ba_3Si_5O_{13}$ and 1.85 wt% $BaSi_2O_5$ was synthesised, and the $BaSi_2O_5$-$Ba_3Si_5O_{13}$ system could be obtained in $BaSi_xO_{1+2x}$ ($1.68 \leq x \leq 1.69$) ceramics. With the further increase in x, the other $Ba_5Si_8O_{21}$ second phase appeared in $BaSi_xO_{1+2x}$ ($1.7 \leq x \leq 1.90$) ceramics, and the content of the $BaSi_2O_5$ phase increased gradually. Lastly, the results of the Rietveld refinement indicated that the coexistence of the $Ba_5Si_8O_{21}$ and $Ba_3Si_5O_{13}$ phases were obtained in $BaSi_xO_{1+2x}$ ($1.61 \leq x \leq 1.67$) ceramics ($Ba_5Si_8O_{21}$–$Ba_3Si_5O_{13}$ system), and the $Ba_3Si_5O_{13}$ single-phase ceramics could be synthesised in $BaSi_xO_{1+2x}$ ($1.67 < x < 1.68$) ceramics. The phase compositions of the $BaSi_xO_{1+2x}$ ceramics was significantly affected by the ratio of Ba:Si.

As shown in Figure 3 and S1, the thermally etched SEM and EDS map scanning images of $BaSi_xO_{1+2x}$ ($1.61 \leq x \leq 1.90$) ceramics were obtained. The dense and smooth microstructures of $BaSi_xO_{1+2x}$ ($1.61 \leq x \leq 1.90$) ceramics were observed. Only the grains of barium silicates were observed in $BaSi_xO_{1+2x}$ ($1.61 \leq x \leq 1.90$) ceramics. However, the similar monoclinic structure and elemental composition caused difficulty in distinguishing the grains of $Ba_5Si_8O_{21}$ and $Ba_3Si_5O_{13}$ based on Figure 3 and S1. In Figure 3e, the EDS results of Spots A and B indicated that the strip-shaped (Spot B) and large (Spot A) grains were $Ba_3Si_5O_{13}$ and $BaSi_2O_5$, respectively. The $Ba_3Si_5O_{13}$ second phase can be observed in Figure 3f. With the increase in x, the content of strip-shaped grains decreased gradually and the average grain sizes increased, which implies that the content of $BaSi_2O_5$ rose gradually.

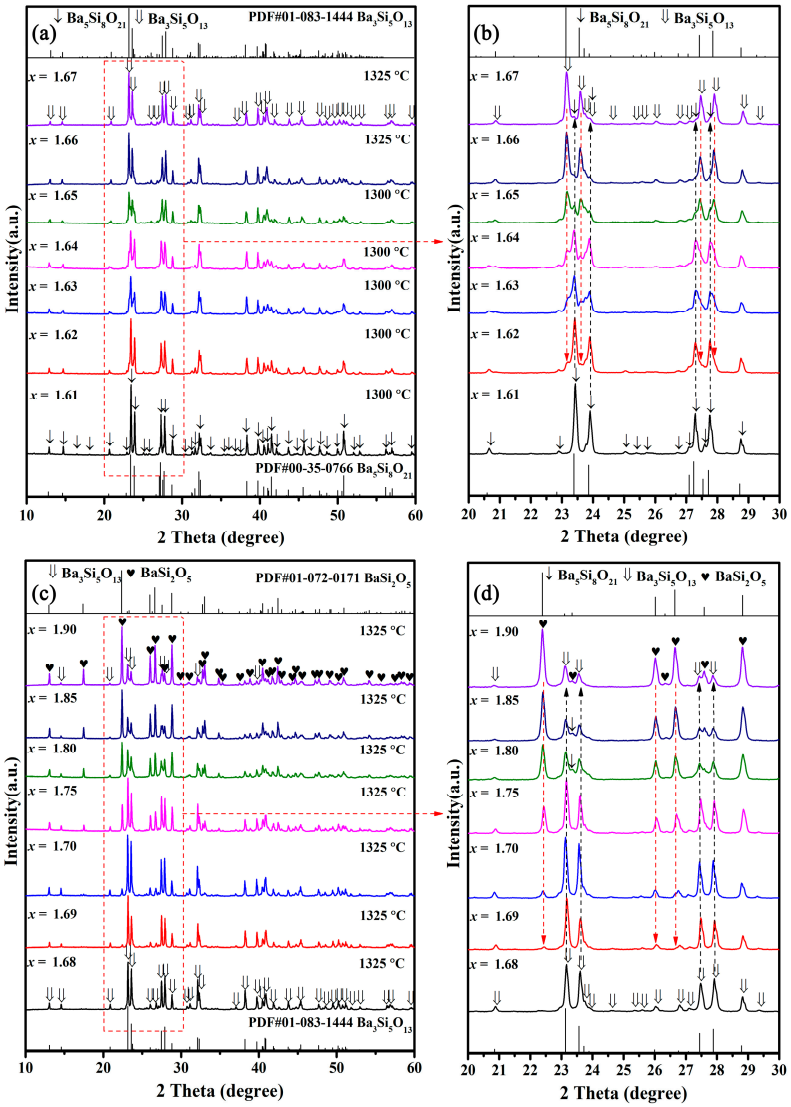


Figure 1. XRD patterns of $BaSi_xO_{1+2x}$ ($1.61 \leq x \leq 1.90$) ceramics sintered at their densification temperature: (**a**) the XRD patterns of $BaSi_xO_{1+2x}$ ($1.61 \leq x \leq 1.67$) ceramics; (**b**) the enlarged XRD patterns of $BaSi_xO_{1+2x}$ ($1.61 \leq x \leq 1.67$) ceramics at 20°~30°; (**c**) the XRD patterns of $BaSi_xO_{1+2x}$ ($1.68 \leq x \leq 1.90$) ceramics; (**d**) the enlarged XRD patterns of $BaSi_xO_{1+2x}$ ($1.68 \leq x \leq 1.90$) ceramics at 20°~30°.

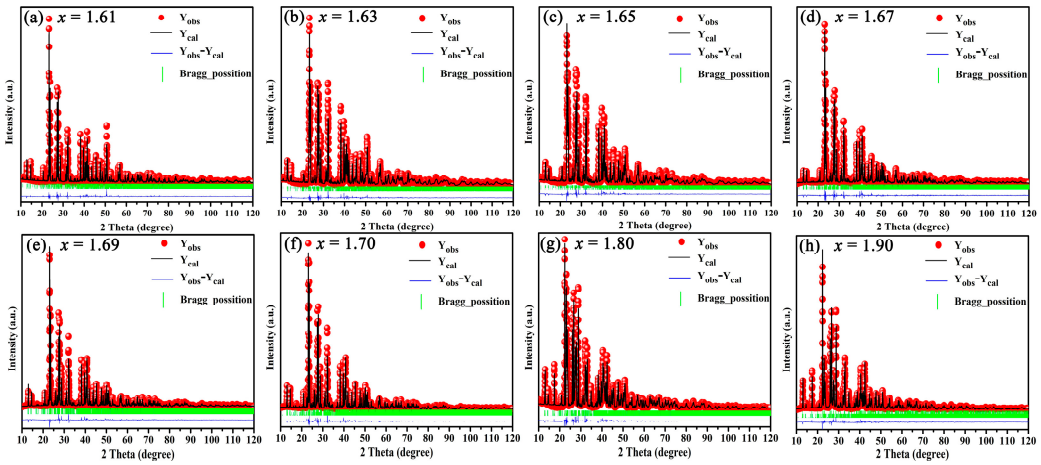


Figure 2. XRD patterns of $BaSi_xO_{1+2x}$ ($1.61 \leq x \leq 1.90$) ceramics after whole XRD pattern fitting.

Table 1. The lattice parameters and Rietveld discrepancy factors of $BaSi_xO_{1+2x}$ ($1.61 \leq x \leq 1.90$) ceramics sintered at their densification temperatures.

Compositions	Phase Compositions		Lattice Parameter of Main Phase					Rietveld Discrepancy Factors		
	Main Phase (wt%)	Second Phase (wt%)	*a* (Å)	*b* (Å)	*c* (Å)	*β* (°)	*V* (Å^3)	R_{wp} (%)	R_p (%)	χ^2
x = 1.61	$Ba_5Si_8O_{21}$ (95.87)	$Ba_3Si_5O_{13}$ (4.13)	32.702	4.698	13.899	98.157	2113.719	16.2	12.9	5.8
x = 1.62	$Ba_5Si_8O_{21}$ (81.66)	$Ba_3Si_5O_{13}$ (18.34)	32.723	4.701	13.892	98.211	2115.226	14.5	11.5	4.8
x = 1.63	$Ba_5Si_8O_{21}$ (70.05)	$Ba_3Si_5O_{13}$ (29.95)	32.741	4.703	13.886	98.299	2115.890	16.5	12.8	6.1
x = 1.64	$Ba_5Si_8O_{21}$ (57.21)	$Ba_3Si_5O_{13}$ (42.79)	32.730	4.701	13.898	98.189	2116.584	16.7	13.1	6.7
x = 1.65	$Ba_3Si_5O_{13}$ (72.70)	$Ba_5Si_8O_{21}$ (27.30)	20.196	4.710	13.866	98.697	1303.919	15.7	12.1	5.3
x = 1.66	$Ba_3Si_5O_{13}$ (85.75)	$Ba_5Si_8O_{21}$ (14.25)	20.199	4.710	13.858	98.657	1303.376	13.7	10.4	4.2
x = 1.67	$Ba_3Si_5O_{13}$ (91.27)	$Ba_5Si_8O_{21}$ (8.73)	20.208	4.710	13.854	98.639	1303.641	13.6	10.8	3.7
x = 1.68	$Ba_3Si_5O_{13}$ (98.15)	$BaSi_2O_5$ (1.85)	20.213	4.712	13.856	98.617	1304.856	14.2	10.9	4.4
x = 1.69	$Ba_3Si_5O_{13}$ (96.99)	$BaSi_2O_5$ (3.01)	20.212	4.711	13.855	98.620	1304.388	14.0	10.9	4.0
x = 1.70	$Ba_3Si_5O_{13}$ (92.64)	$BaSi_2O_5$ (4.68) $Ba_5Si_8O_{21}$ (2.68)	20.210	4.711	13.853	98.617	1304.110	14.5	11.0	5.0
x = 1.75	$Ba_3Si_5O_{13}$ (67.58)	$BaSi_2O_5$ (26.83) $Ba_5Si_8O_{21}$ (5.59)	20.213	4.712	13.854	98.611	1304.643	13.7	10.7	4.9
x = 1.8	$BaSi_2O_5$ (41.79)	$Ba_3Si_5O_{13}$ (41.34) $Ba_5Si_8O_{21}$ (16.87)	4.633	7.689	13.515	—	481.480	13.7	10.6	5.2
x = 1.85	$BaSi_2O_5$ (61.07)	$Ba_3Si_5O_{13}$ (26.28) $Ba_5Si_8O_{21}$ (12.65)	4.634	7.688	13.524	—	481.766	14.0	11.0	5.2
x = 1.9	$BaSi_2O_5$ (71.12)	$Ba_3Si_5O_{13}$ (28.36) $Ba_5Si_8O_{21}$ (0.52)	4.635	7.688	13.527	—	482.064	11.9	9.3	3.8

The microwave dielectric properties of the $BaSi_xO_{1+2x}$ ($1.61 \leq x \leq 1.90$) ceramics sintered at the optimal temperature were obtained, as shown in Table S1 (see Supplementary materials) and Figures 4 and 5. As shown in Figure 4a, the relative density (ρ_{rel}) and experimental relative permittivity ($\varepsilon_{r\text{-exp}}$) of $BaSi_xO_{1+2x}$ ($1.61 \leq x \leq 1.90$) ceramics fluctuated with the increase in x, and all $BaSi_xO_{1+2x}$ ($1.61 \leq x \leq 1.90$) ceramics exhibited high ρ_{rel} (>95%) except th $BaSi_xO_{1+2x}$ (x = 1.75) ceramics. Therefore, ρ_{rel} might have little effect on themicrowave dielectric properties of $BaSi_xO_{1+2x}$ ceramics. In the $BaSi_xO_{1+2x}$ ($1.61 \leq x \leq 1.67$) ceramics, the $BaSi_xO_{1+2x}$ (x = 1.67) ceramics with a 91.27 wt% $Ba_3Si_5O_{13}$ phase exhibited the largest

ε_r-exp value, and a low ε_r-exp (7.33) was obtained in $BaSi_xO_{1+2x}$ (x = 1.61) ceramics with a 95.87 wt% $Ba_5Si_8O_{21}$ phase, which was attributed to the low ε_r-exp value (7.3) of $Ba_5Si_8O_{21}$ ceramics [9]. In $BaSi_xO_{1+2x}$ ($1.68 \leq x \leq 1.90$) ceramics, ε_r-exp decreased from 7.49 to 6.94, and the $BaSi_xO_{1+2x}$ (x = 1.90) ceramics with a 71.12 wt% $BaSi_2O_5$ phase exhibited the lowest ε_r-exp value. For multi-phase ceramics, ε_r could be calculated using the Lichtenecker empirical rule [26–28].

$$ln\ \varepsilon_{r-cal} = V_1\ ln\ \varepsilon_{r-1} + V_2\ ln\ \varepsilon_{r-2} + V_3\ ln\ \varepsilon_{r-3} \quad (1)$$

where $\varepsilon_{r\text{-}cal}$ represents the calculated relative permittivity; V_1, V_2 and V_3 are the volume fraction of phases 1, 2 and 3; and $\varepsilon_{r\text{-}1}$, $\varepsilon_{r\text{-}2}$ and $\varepsilon_{r\text{-}3}$ are the ε_r-exp values of $Ba_5Si_8O_{21}$, $Ba_3Si_5O_{13}$ and $BaSi_2O_5$ ceramics [9], respectively. The $\varepsilon_{r\text{-}cal}$ of $BaSi_xO_{1+2x}$ ($1.61 \leq x \leq 1.90$) ceramics increased initially and then decreased, and the variation tendency of the ε_r-exp values was similar to $\varepsilon_{r\text{-}cal}$ with x (Figure 4a). This finding implies that phase compositions significantly affected the ε_r-exp values for $BaSi_xO_{1+2x}$ ($1.61 \leq x \leq 1.90$) ceramics. Moreover, the $BaSi_xO_{1+2x}$ (x = 1.66) ceramics exhibited lower ε_r-exp (7.57) than $BaSi_xO_{1+2x}$ (x = 1.64, 1.65, 1.67) ceramics, which was attributed to their low ρ_{rel}. The $BaSi_xO_{1+2x}$ (x = 1.80) ceramics exhibited larger ρ_{rel} and ε_r-exp than $BaSi_xO_{1+2x}$ (x = 1.75) ceramics. Thus, the effect of ρ_{rel} on the ε_r-exp of $BaSi_xO_{1+2x}$ ($1.61 \leq x \leq 1.90$) ceramics cannot be neglected.

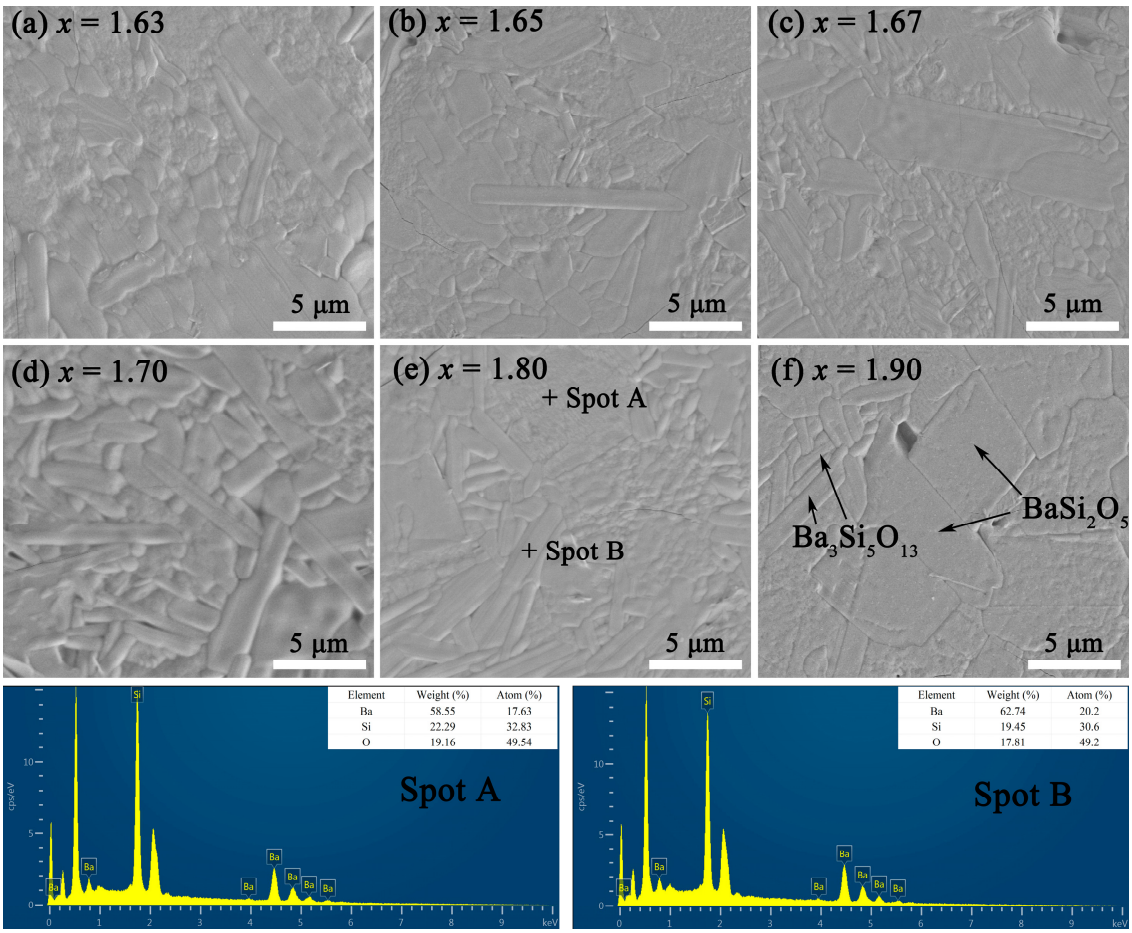


Figure 3. SEM and EDS images of thermally etched $BaSi_xO_{1+2x}$ ($1.61 \leq x \leq 1.90$) ceramics.

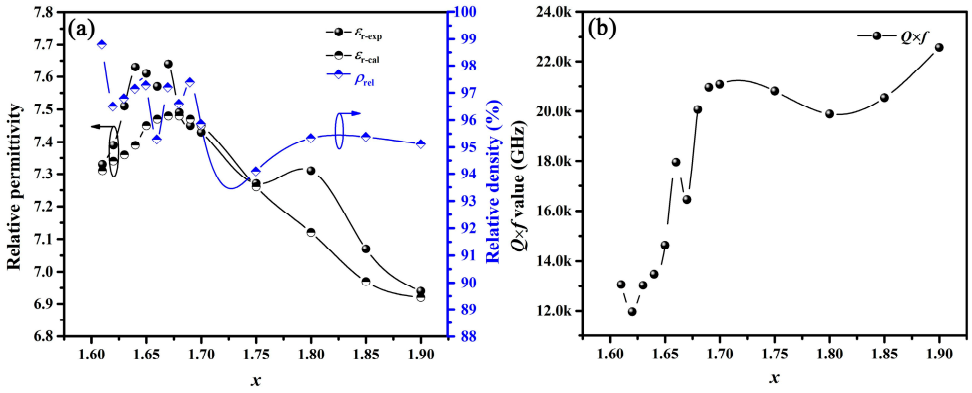


Figure 4. (**a**) Variation in $\varepsilon_{r\text{-exp}}$, ρ_{rel} and $\varepsilon_{r\text{-}cal}$ of $BaSi_xO_{1+2x}$ ($1.61 \leq x \leq 1.90$) ceramics with x; (**b**) variation in $Q \times f$ values of $BaSi_xO_{1+2x}$ ($1.61 \leq x \leq 1.90$) ceramics with x.

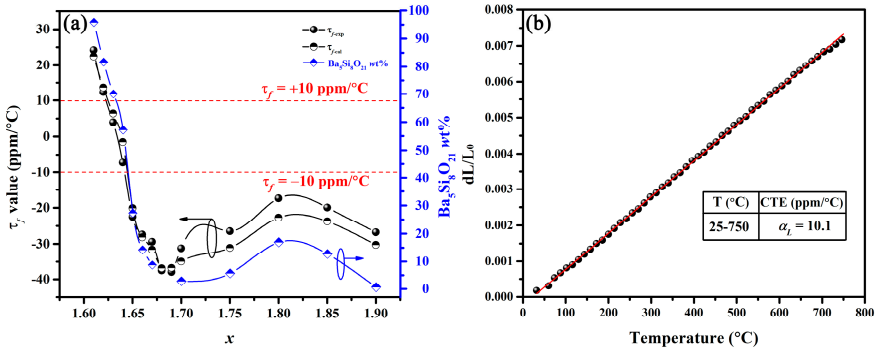


Figure 5. (**a**) Variation in $\tau_{f\text{-exp}}$, $\tau_{f\text{-}cal}$ and $Ba_5Si_8O_{21}$ wt% of $BaSi_xO_{1+2x}$ ($1.61 \leq x \leq 1.90$) ceramics with x; (**b**) thermal expansion of $BaSi_xO_{1+2x}$ ($x = 1.63$) ceramics.

Figure 4b shows the $Q \times f$ values of $BaSi_xO_{1+2x}$ ($1.61 \leq x \leq 1.90$) ceramics. The $BaSi_xO_{1+2x}$ ($1.68 \leq x \leq 1.90$) ceramics exhibited higher $Q \times f$ values than $BaSi_xO_{1+2x}$ ($1.61 \leq x \leq 1.67$) ceramics, and the $BaSi_xO_{1+2x}$ ($x = 1.90$) ceramics with 71.12 wt% $BaSi_2O_5$ phase exhibited high $Q \times f$ value (22,563 GHz), which was attributed to the high $Q \times f$ value of $BaSi_2O_5$ ceramics [9]. Moreover, the low $Q \times f$ value of $BaSi_xO_{1+2x}$ ($x = 1.80$) ceramics was obtained at $1.68 \leq x \leq 1.90$. This result indicates that the largest harmful inner stress at the two-phase interface was obtained in $BaSi_xO_{1+2x}$ ($x = 1.80$) ceramics with 41.79 wt% $BaSi_2O_5$ phase, 41.34 wt% $Ba_3Si_5O_{13}$ phase and 16.87 wt% $Ba_5Si_8O_{21}$ phase. The inner stress at the two-phase interface could not be neglected in multiphase $BaSi_xO_{1+2x}$ ($1.61 \leq x \leq 1.90$) ceramics. The $BaSi_xO_{1+2x}$ ($x = 1.61$) ceramics with minimal $Ba_3Si_5O_{13}$ phase (4.13 wt%) exhibited lower $Q \times f$ value (13,062 GHz) than $Ba_5Si_8O_{21}$ single-phase ceramics (16,700 GHz) due to the existence of inner stress at the two-phase interface. The $Q \times f$ value of $BaSi_xO_{1+2x}$ ($x = 1.68$) ceramics with a 98.15 wt% $Ba_3Si_5O_{13}$ phase was higher than that of $BaSi_xO_{1+2x}$ ($1.61 \leq x \leq 1.67$) ceramics, which means that $Ba_3Si_5O_{13}$ ceramics might exhibit higher $Q \times f$ value than $Ba_5Si_8O_{21}$ ceramics.

The $\tau_{f\text{-exp}}$ values of $BaSi_xO_{1+2x}$ ($1.61 \leq x \leq 1.90$) ceramics were obtained, as shown in Figure 5a. At $1.61 \leq x \leq 1.67$ ($Ba_5Si_8O_{21}$-$Ba_3Si_5O_{13}$ system), the $\tau_{f\text{-exp}}$ values changed from +24.20 ppm/°C to −29.40 ppm/°C, and the $BaSi_xO_{1+2x}$ ($x = 1.63$ and 1.64) ceramics exhibited near-zero $\tau_{f\text{-exp}}$ values. At $1.68 \leq x \leq 1.90$, the $\tau_{f\text{-exp}}$ values of the $BaSi_xO_{1+2x}$ ceramics fluctuated with x, and the small $|\tau_{f\text{-exp}}|$ value was obtained at $x = 1.80$. For multi-phase ceramics, $\tau_{f\text{-}cal}$ could be calculated using Lichtenecker's empirical rule [26–28].

$$\tau_{f-cal} = V_1\tau_{f1} + V_2\tau_{f2} + V_3\tau_{f3} \quad (2)$$

where $\tau_{f\text{-}cal}$ represents the calculated τ_f; V_1, V_2 and V_3 are the volume fractions of phases 1, 2 and 3, respectively; and τ_{f1}, τ_{f2} and τ_{f3} are the τ_f values of $Ba_5Si_8O_{21}$, $Ba_3Si_5O_{13}$ and $BaSi_2O_5$ ceramics [9], respectively. $\tau_{f\text{-}cal}$ agreed well with the $\tau_{f\text{-exp}}$ in $BaSi_xO_{1+2x}$

($1.61 \leq x \leq 1.90$) ceramics, and $\tau_{f\text{-exp}}$, $\tau_{f\text{-}cal}$ and content of $Ba_5Si_8O_{21}$ phase of the $BaSi_xO_{1+2x}$ ($1.61 \leq x \leq 1.90$) ceramics with x displayed a similar trend. Therefore, the content of the $Ba_5Si_8O_{21}$ phase significantly affected the $\tau_{f\text{-exp}}$ of $BaSi_xO_{1+2x}$ ($1.61 \leq x \leq 1.90$) ceramics. At $1.65 \leq x \leq 1.75$, the $BaSi_xO_{1+2x}$ ceramics with the $Ba_3Si_5O_{13}$ main phase exhibited negative $\tau_{f\text{-exp}}$ values. Therefore, the present study confirmed the negative τ_f value of $Ba_3Si_5O_{13}$ ceramics, which was controversial in a previous work [9]. $Ba_5Si_8O_{21}$, as a new τ_f compensator, successfully adjusted the negative $\tau_{f\text{-exp}}$ value of $Ba_3Si_5O_{13}$ to near zero (+3.95 ppm/°C and −7.25 ppm/°C) in the $BaSi_xO_{1+2x}$ (x = 1.63, 1.64) ceramics.

In accordance with Formula (3) [29,30], the τ_f related to α_L and τ_ε and α_L can be seen in Figure 5b.

$$\tau_f = -\left(\alpha_L + \frac{1}{2}\tau_\varepsilon\right) \quad (3)$$

with the increase in measured temperature, the length of $BaSi_xO_{1+2x}$ (x = 1.63) ceramics increased gradually, and the average linear thermal expansion coefficient (CTE in Figure 5b) at 25–750 °C is 10.1 ppm/°C. The dependence of ε_r on temperature for $BaSi_xO_{1+2x}$ ($1.61 \leq x \leq 1.90$) ceramics is shown in Figure 6, and the fitting τ_ε values at 30–125 °C and 1 MHz were obtained. The negative τ_ε values were obtained in $BaSi_xO_{1+2x}$ ($1.61 \leq x \leq 1.64$) ceramics, and $BaSi_xO_{1+2x}$ ($1.66 \leq x \leq 1.90$) ceramics exhibited positive τ_ε values. At $1.61 \leq x \leq 1.64$, the negative τ_ε values increased gradually to near zero, and $BaSi_xO_{1+2x}$ (x = 1.64) ceramics exhibited a near-zero τ_ε value (−2.9 ppm/°C). At $1.66 \leq x \leq 1.90$, the small τ_ε value was obtained in $BaSi_xO_{1+2x}$ (x = 1.80) ceramics. According to the τ_f–ε_r relationship, a similar variation in the τ_ε and τ_f values of the $BaSi_xO_{1+2x}$ ($1.61 \leq x \leq 1.90$) ceramics was observed as x increased, which indicates that the measured $\tau_{f\text{-exp}}$ values using the Hakki–Coleman method were exacted. The measured α_L (10.1 ppm/°C) and τ_ε (−15.4 ppm/°C) values of $BaSi_xO_{1+2x}$ (x = 1.63) ceramics also confirmed their near-zero $\tau_{f\text{-exp}}$ value.

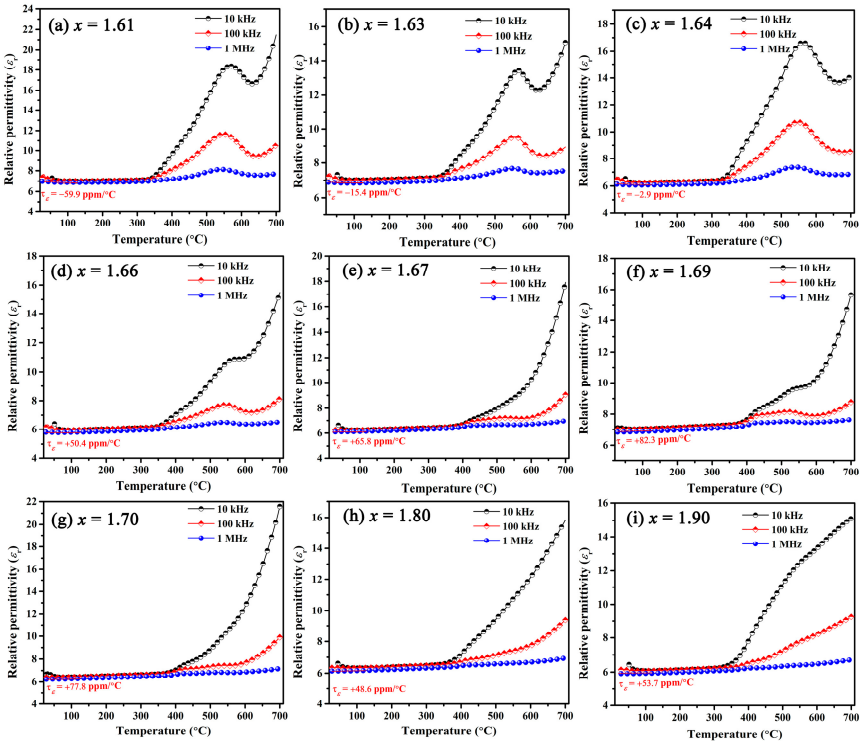


Figure 6. Temperature and frequency dependences of relative permittivity for $BaSi_xO_{1+2x}$ ($1.61 \leq x \leq 1.90$) ceramics.

At high T_{sint} (≥1300 °C), the phase compositions of $BaSi_xO_{1+2x}$ ($1.61 \leq x \leq 1.90$) ceramics were revealed in this work. However, the phase compositions of barium silicates were sensitive to T_{sint}, and the complex phase transformation of barium silicates existed

with the change in T_{sint}, especially $Ba_5Si_8O_{21}$, $Ba_3Si_5O_{13}$ and $BaSi_2O_5$ ceramics [9,10]. Thus, the phase transformation of $BaSi_xO_{1+2x}$ ceramics with the change in T_{sint} must be clarified. The $BaSi_xO_{1+2x}$ ($x = 1.63$) ceramics sintered at 1300 °C presented the coexistence of $Ba_5Si_8O_{21}$ and $Ba_3Si_5O_{13}$ phases and exhibited good microwave dielectric properties. As shown in Figure 7, the XRD patterns of $BaSi_{1.63}O_{4.26}$-y wt% LiF ($1 \leq y \leq 3$) ceramics were obtained. The coexistence of $Ba_5Si_8O_{21}$ and $BaSi_2O_5$ phases was obtained in $BaSi_{1.63}O_{4.26}$-1 wt% LiF ceramics sintered at 1025 °C, and the $Ba_3Si_5O_{13}$ second phase of $BaSi_{1.63}O_{4.26}$ ceramics sintered at 1300 °C was inhibited. However, the new $Ba_2Si_3O_8$ and SiO_2 second phases appeared in $BaSi_{1.63}O_{4.26}$-1 wt% LiF ceramics when T_{sint} = 925 °C, which implies that the $Ba_2Si_3O_8$ and SiO_2 phase can transform into $BaSi_2O_5$ phases at T_{sint} = 1025 °C. With the increase in the content of LiF, the T_{sint} of $BaSi_{1.63}O_{4.26}$-y wt% LiF ($1 \leq y \leq 3$) ceramics decreased gradually. The coexistence of $Ba_5Si_8O_{21}$, $Ba_2Si_3O_8$, $BaSi_2O_5$ and SiO_2 phases was observed in $BaSi_{1.63}O_{4.26}$-y wt% LiF (y = 2, 3) ceramics sintered at 925 and 800 °C.

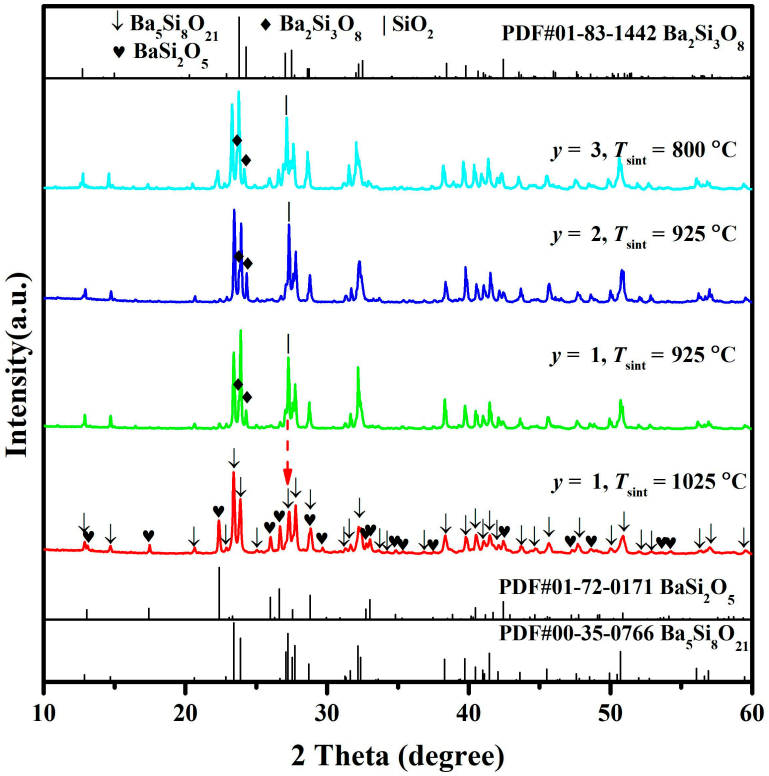


Figure 7. XRD patterns of $BaSi_{1.63}O_{4.26}$-y wt% LiF ($1 \leq y \leq 3$) ceramics at different sintering temperatures.

Figure S2 and Table 2 show the results of Rietveld refinement. The calculated XRD patterns of $BaSi_{1.63}O_{4.26}$-y wt% LiF ($1 \leq y \leq 3$) ceramics matched the measured XRD patterns well (Figure S2). The phase compositions of $BaSi_{1.63}O_{4.26}$-y wt% LiF ($1 \leq y \leq 3$) ceramics were observed, as shown in Table 2. The $BaSi_{1.63}O_{4.26}$-1 wt% LiF ceramics with 74.39 wt% $Ba_5Si_8O_{21}$ and 25.61 wt% $BaSi_2O_5$ phases was obtained. The decrease in T_{sint} induced the appearance of the $Ba_2Si_3O_8$ second phase, and 84.51 wt% and 68.69 wt% $Ba_5Si_8O_{21}$ phases were obtained in $BaSi_{1.63}O_{4.26}$-y wt% LiF (y = 2, 3) ceramics. The $Ba_3Si_5O_{13}$ phase could not be obtained in $BaSi_{1.63}O_{4.26}$-y wt% LiF ($1 \leq y \leq 3$) ceramics with low T_{sint} (≤1025 °C), which means that $Ba_3Si_5O_{13}$ phase can only be synthesised at high T_{sint} (≥1300 °C). The $Ba_5Si_8O_{21}$, $Ba_2Si_3O_8$ and $BaSi_2O_5$ phases can be synthesised at low T_{sint} (≤925 °C). In summary, the $Ba_5Si_8O_{21}$ phase was the most stable phase of barium silicates, and the phase compositions of $BaSi_{1.63}O_{4.26}$-y wt% LiF ($1 \leq y \leq 3$) ceramics were related to T_{sint}.

Table 2. The lattice parameters and Rietveld discrepancy factors of $BaSi_{1.63}O_{4.26}$-*y* wt% LiF ($1 \leq y \leq 3$) ceramics sintered at their densification temperatures.

Compositions	Phase Compositions		Lattice Parameter of Main Phase					Rietveld Discrepancy Factors		
	Main Phase (wt%)	Second Phase (wt%)	*a* (Å)	*b* (Å)	*c* (Å)	*β* (°)	*V* (Å^3)	R_{wp} (%)	R_p (%)	χ^2
y = 1	$Ba_5Si_8O_{21}$ (74.39)	$BaSi_2O_5$ (25.61)	32.687	4.694	13.877	98.276	2106.951	12.0	9.1	3.9
y = 2	$Ba_5Si_8O_{21}$ (84.51)	$Ba_2Si_3O_8$ (13.14) $BaSi_2O_5$ (1.10) SiO_2 (1.25)	32.699	4.699	13.900	98.155	2114.038	18.3	14.5	7.6
y = 3	$Ba_5Si_8O_{21}$ (68.69)	$Ba_2Si_3O_8$ (15.55) $BaSi_2O_5$ (13.70) SiO_2 (2.06)	32.697	4.697	13.898	98.159	2112.718	16.0	12.6	6.5

The thermally etched SEM images of $BaSi_{1.63}O_{4.26}$-3 wt% LiF and $BaSi_{1.63}O_{4.26}$-3 wt% LiF-Ag electrode ceramics were obtained, as shown in Figure 8. Dense and smooth microstructures were observed in $BaSi_{1.63}O_{4.26}$-3 wt% LiF ceramics. The evident small SiO_2 second phase existed at the grain boundary, as shown in Figures 8 and S3. No LiF or liquid phases existed, and complex phase compositions could not be clarified via SEM images. As shown in Figure 8b, the surface of $BaSi_{1.63}O_{4.26}$-3 wt% LiF ceramics could be well combined with Ag electrodes, which indicates that it is well able be co-fired with Ag electrodes at 800 °C.

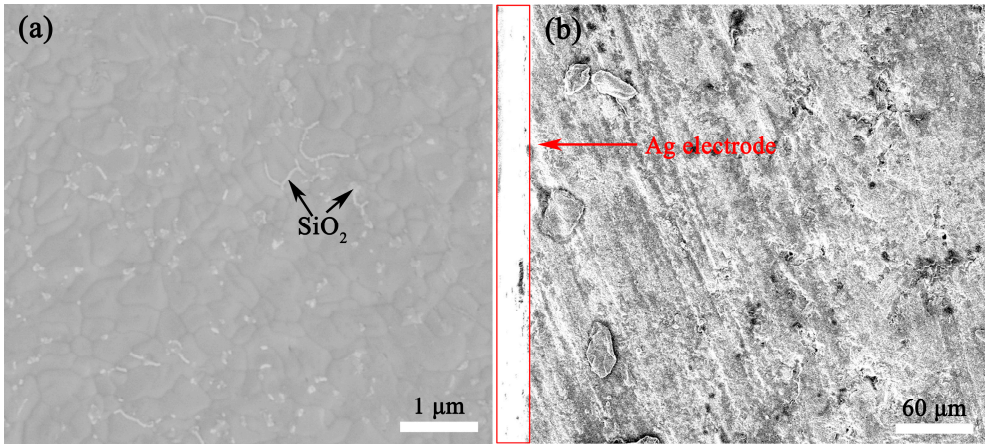


Figure 8. SEM images of the thermally etched (**a**) $BaSi_{1.63}O_{4.26}$-3 wt% LiF ceramics and (**b**) $BaSi_{1.63}O_{4.26}$-3 wt% LiF-Ag electrode ceramics.

The evolution of the phase compositions and sintering characteristic of $BaSi_{1.63}O_{4.26}$-*y* wt% LiF ($1 \leq y \leq 3$) ceramics on microwave dielectric properties was investigated. As shown in Table 3, with the addition of a LiF sintering aid, the optimal T_{sint} of $BaSi_{1.63}O_{4.26}$-*y* wt% LiF ($1 \leq y \leq 3$) ceramics were able to be reduced to less than 1025 °C. At the optimal sintering temperatures, the ρ_{rel} of $BaSi_{1.63}O_{4.26}$-*y* wt% LiF ($1 \leq y \leq 3$) ceramics decreased from 96.5% (*y* = 1) to 94.4% (*y* = 3), and the addition of a LiF sintering aid [31] and the decrease in sintering temperature caused a reduction in ρ_{rel}. The ε_r-exp and $Q \times f$ values decreased gradually, and the τ_f-exp values fluctuated with *x*. The decrease in ε_r-exp and $Q \times f$ values was mainly attributed to the decline in ρ_{rel}. According to Formula (2), the $\tau_{f\text{-}cal}$ values of $BaSi_{1.63}O_{4.26}$-*y* wt% LiF ($1 \leq y \leq 3$) ceramics were calculated, and similar variations in τ_f-exp, $\tau_{f\text{-}cal}$ and the content of the $Ba_5Si_8O_{21}$ phase of the $BaSi_{1.63}O_{4.26}$-*y* wt%

LiF ($1 \leq y \leq 3$) ceramics were observed as y increased. The $\tau_{f\text{-exp}}$ values of $BaSi_{1.63}O_{4.26}$-y wt% LiF ($1 \leq y \leq 3$) ceramics were significantly affected by the content of the $Ba_5Si_8O_{21}$ phase, and the near-zero $\tau_{f\text{-exp}}$ value (+5.75 ppm/°C) was obtained in $BaSi_{1.63}O_{4.26}$-3 wt% LiF ceramics with 68.69 wt% $Ba_5Si_8O_{21}$, 15.55 wt% $Ba_2Si_3O_8$, 13.70 wt% $BaSi_2O_5$ and 2.06 wt% SiO_2 phases.

Table 3. The optimal sintering temperature, relative density and microwave dielectric properties of $BaSi_{1.63}O_{4.26}$-y wt% LiF ($1 \leq y \leq 3$) ceramics.

Compositions	T_{sint} (°C)	ρ_{rel} (%)	$\varepsilon_{r\text{-exp}}$	$Q \times f$ (GHz)	τ_f (ppm/°C)	$\tau_{f\text{-}cal}$ (ppm/°C)
$y = 1$	1025	96.5	7.42	14,252	+8.37	+11.00
$y = 2$	950	95.2	7.21	12,913	+11.90	+16.20
$y = 3$	800	94.4	7.10	12,463	+5.75	+6.12

4. Conclusions

$BaSi_xO_{1+2x}$ ($1.61 \leq x \leq 1.90$) and $BaSi_{1.63}O_{4.26}$-y wt% LiF ($1 \leq y \leq 3$) ceramics were synthesised, and the evolution of their phase compositions was investigated. The two-phase system of $Ba_5Si_8O_{21}$ and $Ba_3Si_5O_{13}$ was obtained at $1.61 \leq x \leq 1.67$, and no other second phase existed. At $1.67 \leq x \leq 1.69$, the content of $Ba_3Si_5O_{13}$ phase was more than 90 wt%. The $Ba_5Si_8O_{21}$ second phase could be inhibited in $BaSi_xO_{1+2x}$ ($1.68 \leq x \leq 1.69$) ceramics, and the other $BaSi_2O_5$ phase was induced. At $1.70 \leq x \leq 1.90$, the excessive Si element content of $BaSi_xO_{1+2x}$ ceramics caused the appearance of the $Ba_5Si_8O_{21}$ second phase, and the coexistence of $BaSi_2O_5$, $Ba_5Si_8O_{21}$ and $Ba_3Si_5O_{13}$ phases was observed. Therefore, the phase compositions of $BaSi_xO_{1+2x}$ ($1.61 \leq x \leq 1.90$) ceramics sintered at high temperature (≥1300 °C) were significantly controlled by the ratio of Ba:Si. The $\varepsilon_{r\text{-exp}}$ and $Q \times f$ values of $BaSi_xO_{1+2x}$ ($1.61 \leq x \leq 1.90$) ceramics were mainly affected by the phase compositions and ρ_{rel}, and the $\tau_{f\text{-exp}}$ values were controlled via the content of the $Ba_5Si_8O_{21}$ phase with a positive τ_f value. The near-zero $\tau_{f\text{-exp}}$ value (+3.95 ppm/°C) was obtained at $x = 1.63$. Moreover, the LiF sintering aids were able to reduce the sintering temperature of $BaSi_{1.63}O_{4.26}$ ceramics, and the low sintering temperature (800 °C) was obtained in $BaSi_{1.63}O_{4.26}$-y wt% LiF ($y = 3$) ceramics. When sintering temperature was less than 1025 °C, the $Ba_3Si_5O_{13}$ phase of $BaSi_{1.63}O_{4.26}$ ceramics was inhibited and the $Ba_2Si_3O_8$, $BaSi_2O_5$ and SiO_2 appeared. The content of phases could be affected by the sintering temperature, which shows that the phase compositions of $BaSi_xO_{1+2x}$ ceramics were related to their sintering temperature. The development of microwave dielectric properties of $BaSi_{1.63}O_{4.26}$-y wt% LiF ($1 \leq y \leq 3$) ceramics strongly relied on their phase compositions, and microwave dielectric properties ($\varepsilon_r = 7.10$, $Q \times f = 12{,}463$ GHz, and $\tau_f = +5.75$ ppm/°C) were obtained in $BaSi_{1.63}O_{4.26}$-3 wt% LiF ceramics.

Supplementary Materials: The following supporting information can be downloaded at https://www.mdpi.com/article/10.3390/cryst13060870/s1, Figure S1: EDS map scanning images of the thermally etched $BaSi_xO_{1+2x}$ ($x = 1.67$ and 1.80) ceramics; Figure S2: XRD patterns of $BaSi_{1.63}O_{4.26}$-y wt% LiF ($1 \leq y \leq 3$) ceramics after whole XRD pattern fitting; Figure S3: EDS map scanning images of the thermally etched $BaSi_{1.63}O_{4.26}$-3 wt% LiF ceramics; Table S1: Optimal sintered temperature (T_{sint}), relative density (ρ_{rel}) and microwave dielectric properties of $BaSi_xO_{1+2x}$ ($1.61 \leq x \leq 1.90$) ceramics.

Author Contributions: Conceptualization, T.W. and Y.L.; methodology, Z.Z.; software, X.L. (Xiaotian Liu); validation, X.L. (Xiaoxiao Li); formal analysis, T.W.; investigation, K.D.; resources, K.D.; data curation, T.W.; writing—original draft preparation, K.D.; writing—review and editing, K.D. and W.L.; visualization, Y.L.; supervision, C.Y.; project administration, Y.C.; funding acquisition, W.L. and S.W. All authors have read and agreed to the published version of the manuscript.

Funding: This work was financially supported by the Natural Science Foundation of China grant number 52072133.

Data Availability Statement: Data is unavailable due to privacy.

Conflicts of Interest: The authors declare no conflict of interest.

References

1. Zhou, D.; Pang, L.X.; Wang, D.W.; Li, C.; Jin, B.B.; Reaney, I.M. High permittivity and low loss microwave dielectrics suitable for 5G resonators and low temperature co-fired ceramic architecture. *J. Mater. Chem. C* **2017**, *5*, 10094–10098. [CrossRef]
2. Wu, F.F.; Zhou, D.; Du, C.; Jin, B.B.; Li, C.; Qi, Z.M. Design of a Sub-6 GHz dielectric resonator antenna with novel temperature-stabilized $(Sm_{1-x}Bi_x)NbO_4$ (x = 0–0.15) microwave dielectric ceramics. *ACS Appl. Mater. Inter.* **2022**, *14*, 7030–7038. [CrossRef] [PubMed]
3. Yin, C.Z.; Yu, Z.Z.; Shu, L.L.; Liu, L.J.; Chen, Y.; Li, C.C. A low-firing melilite ceramic $Ba_2CuGe_2O_7$ and compositional modulation on microwave dielectric properties through Mg substitution. *J. Adv. Ceram.* **2021**, *10*, 108–119. [CrossRef]
4. Tian, H.R.; Zheng, J.J.; Liu, L.T.; Wu, H.T.; Kimura, H.; Lu, Y.Z. Structure characteristics and microwave dielectric properties of $Pr_2(Zr_{1-x}Ti_x)_3(MoO_4)_9$ solid solution ceramic with a stable temperature coefficient. *J. Mater. Sci. Technol.* **2022**, *116*, 121–129. [CrossRef]
5. Liu, L.T.; Chen, Y.G.; Feng, Z.B.; Wu, H.T.; Zhang, X.Y. Crystal structure, infrared spectra, and microwave dielectric properties of the $EuNbO_4$ ceramic. *Ceram Int.* **2021**, *47*, 4321–4326. [CrossRef]
6. Grebenschikov, R.G.; Toropov, N.A. New data on the barium oxide-silica phase diagram. *Izvest. Akad. Nauk. SSSR Ser. Chem.* **1962**, *11*, 545–553.
7. Zhang, R.L.; Maeda, T.; Maruta, R.; Kusaka, S.; Ding, B.J.; Murai, K.I. Luminescence enhancement of Eu^{2+}, Ce^{3+} co-doped $Ba_3Si_5O_{13-\delta}N_\delta$ phosphors. *J. Solid State Chem.* **2010**, *183*, 620–623. [CrossRef]
8. Gorelova, L.A.; Bubnova, R.S.; Krivovichev, S.V.; Krzhizhanovskaya, M.G.; Filatov, S.K. Thermal expansion and structural complexity of Ba silicates with tetrahedrally coordinated Si atoms. *J. Solid State Chem.* **2016**, *235*, 76–84. [CrossRef]
9. Lei, W.; Zou, Z.Y.; Chen, Z.H.; Ullah, B.; Zeb, A.; Lan, X.K. Controllable τ_f value of barium silicate microwave dielectric ceramics with different Ba/Si ratios. *J. Am. Ceram. Soc.* **2018**, *101*, 25–30. [CrossRef]
10. Wu, P.; Yang, H.Y.; Yang, H.C.; Gui, L.; Wang, Y.C.; Liu, Q. Synthesis of a low-firing $BaSi_2O_5$ microwave dielectric ceramics with low dielectric constant. *Ceram. Int.* **2022**, *48*, 17289–17297. [CrossRef]
11. Zhang, Y.; Li, X.N.; Ding, S.H.; Song, T.X.; Yin, Z.Z.; Dan, J.Y. Crystal structure and microwave dielectric properties of Li-modified $BaSi_2O_5$ ceramics. *J. Mater. Res. Technol.* **2023**, *22*, 2792–2805. [CrossRef]
12. Song, X.Q.; Du, K.; Zou, Z.Y.; Chen, Z.H.; Lu, W.Z.; Wang, S.H. Temperature-stable $BaAl_2Si_2O_8$–$Ba_5Si_8O_{21}$-based low-permittivity microwave dielectric ceramics for LTCC applications. *Ceram. Int.* **2017**, *43*, 14453–14456. [CrossRef]
13. Joseph, T.; Sebastian, M.T. Microwave dielectric properties of alkaline earth orthosilicates M_2SiO_4 (M = Ba, Sr, Ca). *Mater. Lett.* **2011**, *65*, 891–893. [CrossRef]
14. Wang, D.W.; Ding, L.F.; Heng, B.; Zhu, H.K.; Ding, X.F.; Wang, Z.F. Temperature-stable crystal structure and microwave dielectric properties of $BaSi_2O_5$-$Ba_3V_2O_8$ composite ceramics. *J. Alloys Compd.* **2022**, *927*, 167096–167104. [CrossRef]
15. Du, K.; Song, X.Q.; Zou, Z.Y.; Fan, J.; Lu, W.Z.; Lei, W. Improved microwave dielectric properties of novel low-permittivity Sn-doped $Ca_2HfSi_4O_{12}$ ceramics. *Mater. Res. Bull.* **2020**, *129*, 110887. [CrossRef]
16. Wu, S.P.; Jiang, C.; Mei, Y.X.; Tu, W.P. Synthesis and microwave dielectric properties of Sm_2SiO_5 ceramics. *J. Am Ceram. Soc.* **2012**, *95*, 37–40. [CrossRef]
17. Ma, Q.; Wu, S.; Jiang, C.; Li, J. Microwave dielectric properties of SnO_2-doped $CaSiO_3$ ceramics. *Ceram. Int.* **2013**, *39*, 2223–2229. [CrossRef]
18. Du, K.; Guo, Y.B.; Wang, F.; Fan, J.; Wang, X.C.; Lu, W.Z. Optimized sintering behavior and microwave dielectric properties of $Ca_{1+2x}SnSi_{2x+y}O_{3+6x+2y}$ by composition modulation. *J. Am. Ceram. Soc.* **2021**, *104*, 974–984. [CrossRef]
19. Du, K.; Yin, C.Z.; Guo, Y.B.; Zhang, C.; Wang, X.C.; Lu, W.Z. Phase transition, Infrared spectra, and microwave dielectric properties of temperature-stable $CaSnSi_{1-x}Ge_xO_5$ ceramics. *Ceram. Int.* **2021**, *47*, 24781–24792. [CrossRef]
20. Qin, J.C.; Liu, Z.F.; Ma, M.S.; Li, Y.X. Machine learning approaches for permittivity prediction and rational design of microwave dielectric ceramics. *J. Mater.* **2021**, *7*, 1284–1293. [CrossRef]
21. Qin, J.C.; Liu, Z.F.; Ma, M.S.; Liu, F.; Qi, Z.M.; Li, Y.X. Structure and microwave dielectric properties of gillespite-type $ACuSi_4O_{10}$ (A = Ca, Sr, Ba) ceramics and quantitative prediction of the $Q\times f$ value via machine learning. *ACS Appl. Mater. Interfaces* **2021**, *13*, 17817–17826. [CrossRef] [PubMed]
22. Kamutzki, F.; Schneider, S.; Barowski, J.; Gurlo, A.; Hanaor, D.A.H. Silicate dielectric ceramics for millimetre wave applications. *J. Eur. Ceram. Soc.* **2021**, *41*, 3879–3894. [CrossRef]
23. Yusa, H.; Sata, N.; Ohishi, Y. Rhombohedral (9R) and hexagonal (6H) perovskites in barium silicates under high pressure. *Am. Miner.* **2007**, *92*, 648–654. [CrossRef]
24. Rietveld, H.M. A profile refinement method for nuclear and magnetic structures. *J. Appl. Cryst.* **1969**, *2*, 65–71. [CrossRef]
25. Hakki, B.W.; Coleman, P.D. A dielectric resonant method of measuring inductive capacitance in the millimeter range. *IEEE Trans. Microw. Theory Technol.* **1960**, *8*, 402–410. [CrossRef]
26. Paladino, A.E. Temperature-compensated $MgTi_2O_5$-TiO_2 dielectrics. *J. Am. Ceram. Soc.* **1971**, *54*, 168–169. [CrossRef]
27. Fukuda, K.; Kitoh, R.; Awai, I. Microwave characteristics of TiO_2-Bi_2O_3 dielectric resonator. *Jpn. J. Appl. Phys.* **1993**, *32*, 4584–4588. [CrossRef]

28. He, H.; Xu, Y. A unified equation for predicting the dielectric constant of a two phase composite. *Appl. Phys. Lett.* **2014**, *104*, 062906. [CrossRef]
29. Zhou, D.; Guo, H.H.; Fu, M.S.; Yao, X.G.; Lin, H.X.; Liu, W.F. Anomalous dielectric behaviour at the monoclinic to tetragonal phase transition in $La(Nb_{0.9}V_{0.1})O_4$. Inorg. *Chem. Front.* **2021**, *8*, 156–163.
30. Du, K.; Yin, C.Z.; Guo, Y.B.; Wang, X.C.; Lu, W.Z.; Lei, W. Phase transition and permittivity stability against temperature of $CaSn_{1-x}Ti_xGeO_5$ ceramics. *J. Eur. Ceram. Soc.* **2022**, *42*, 147–153. [CrossRef]
31. Song, X.Q.; Du, K.; Li, J.; Lan, X.K.; Lu, W.Z.; Wang, X.H. Low-fired fluoride microwave dielectric ceramics with low dielectric loss. *Ceram. Int.* **2019**, *45*, 279–286. [CrossRef]

Disclaimer/Publisher's Note: The statements, opinions and data contained in all publications are solely those of the individual author(s) and contributor(s) and not of MDPI and/or the editor(s). MDPI and/or the editor(s) disclaim responsibility for any injury to people or property resulting from any ideas, methods, instructions or products referred to in the content.